J Musculoskelet Neuronal Interact 2008; 8(4):352-362

38th International Sun Valley Workshop
August 3-6, 2008
Posters

Hylonome

Poster abstracts from the 38th Meeting of the International Sun Valley Workshop on Skeletal Tissue Biology

August 5-6, 2008, Sun Valley, Idaho, USA

Program Chairman: David B. Burr

Abstract No.	Topic
P1-21	Poster abstracts (Authors marked with an asterisk (*) are Recipients of the Alice L. Jee Travel Award)

P-1

Relationship Between Estrogen Deficiency-induced Oral Bone Loss and Systemic Osteoporosis

R.B. Anwar[1], M. Tanaka[1], E.Yamashita[1], N. Watanabe[1], M.N. Ali[1], H. Ohshima[1], S. Ejiri[2]
[1]Department of Tissue Regeneration and Reconstruction, Niigata University Graduate School of Medical and Dental Sciences, Niigata, Japan; [2]Department of Oral Anatomy, Asahi University School of Dentistry, Gifu, Japan
E-mail: a_rezwana@yahoo.com

Introduction: Epidemiological studies have shown that postmenopausal women who do not use estrogen supplements have significantly fewer teeth than those who do[1]. However, the mechanism giving rise to this phenomenon has not yet been elucidated. To clarify the relationship between estrogen deficiency and tooth loss, the microstructural alveolar bone changes of ovariectomized monkeys were analyzed in the canine and molar areas and then compared with their radial and lumbar spine bone mineral densities (BMD).

Results and discussion: 12 adult female cynomolgus monkeys were used in this study and divided into 2 groups of 6 subjects. The test group was ovariectomized (OVX) bilaterally and the controls received sham (SHAM) surgery. Periodic measurements were then made of lumbar vertebral (LV)-BMD using DXA, and the subjects were sacrificed after 76 weeks. The trabecular (Tr)-BMD of the right radii and the Tr and cortical (Cr)-BMDs of the canine distal area and mandibular basal area were measured using pQCT. The microstructures were observed in the molar and canine regions with micro-CT. The loss of alveolar crest height in the canine and second molar region, attrition in the first molar, and the size and number of pores on the alveolar socket walls were evaluated in both canine and molar areas.

OVX showed significant decreases in %-change of LV-BMD compared to SHAM, as well as significantly less Tr and Cr BMDs around the canines. OVX also showed significant increases in the number of enlarged pores in both canine and molar regions, and alveolar crest height loss only around canine area. Canine BMDs significantly correlated with %-change in LV-BMD. The pore count in both regions showed significantly negative correlations with the %-change in LV-BMD, as well as alveolar crest height loss around the canines. In the molar region, alveolar crest height loss and %-change in LV-BMD showed no significant correlations. However, loss of alveolar crest height itself showed a significant correlation with attrition. It suggests that the alveolar crest height loss in the molar region may be caused by aging rather than by estrogen deficiency. Considering that periodontal disease is one of the geriatric diseases and molars are more vulnerable to suffer from it, the periodontal disease might exert some effects on the molar area along with estrogen deficiency[2].

Conclusion: Estrogen deficiency led to low BMD and porotic changes in canine and molar alveolar bone, respectively, and some of these changes correlated with decreased lumbar BMD. These findings suggest that in human patients with severe postmenopausal osteoporosis, the alveolar bone supporting the teeth might also become fragile.

References

1. McGrath C, Bedi R. Why are we "weighting"? An assessment of a self-weighting approach to measuring oral health-related quality of life. Community Dent Oral Epidemiol 2004;32:19-24.
2. Page RC, Schroeder HE. Pathogenesis of inflammatory periodontal disease. A summary of current work. Lab Invest 1976;34:235-49.

The authors have no conflict of interest.

P-2

Fluid Flow Induces an Increase in Cell Strain and Intracellular Calcium Production in Osteocytes

*A.R. Bonivtch[1,3], J. Ling[2], J.X. Jiang[4], M.E. Van Dyke[2], L.F. Bonewald[5], D.P. Nicolella[1]
[1]Mechanics and Materials and [2]Bioengineering, Southwest Research Institute® San Antonio, Texas, USA; [3]Wake Forest Institute for Regenerative Medicine, Winston Salem, North Carolina, USA; [4]Department of Biochemistry, The University of Texas Health Science Center, San Antonio, Texas, USA; [5]School of Dentistry, The University of Missouri Kansas City, Kansas City, Missouri, USA
E-mail: amber.bonivtch@swri.org

Introduction: Osteocytes, which exist individually within the lacunae of bone's trabecular network, comprise 90-95% of all bone cells and function as the tissue's mechanosensors[1,2]. Both mechanical stimulation and fluid flow have been shown to elicit biologic responses from osteocytes[3,4]. However, the amount of strain experienced by osteocytes in response to shear applied via fluid flow has not been quantified and associated with a biologic response. The objective of this study was to quantify the strain experienced by individual osteocytes in response to laminar fluid flow and correlate that strain to the upregulation of intracellular calcium levels in real time.

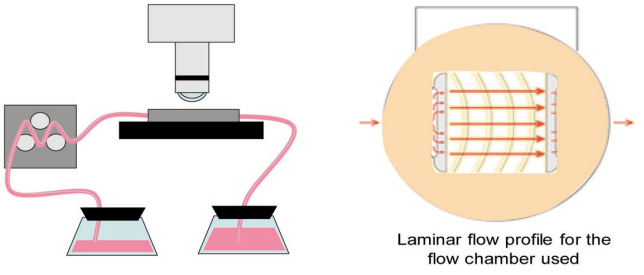

Figure 1. MLO-Y4 cells, seeded on collagen coated glass slides, were loaded with Fluo-4, AM and exposed to laminar fluid flow in a flow chamber attached to a microscope stage.

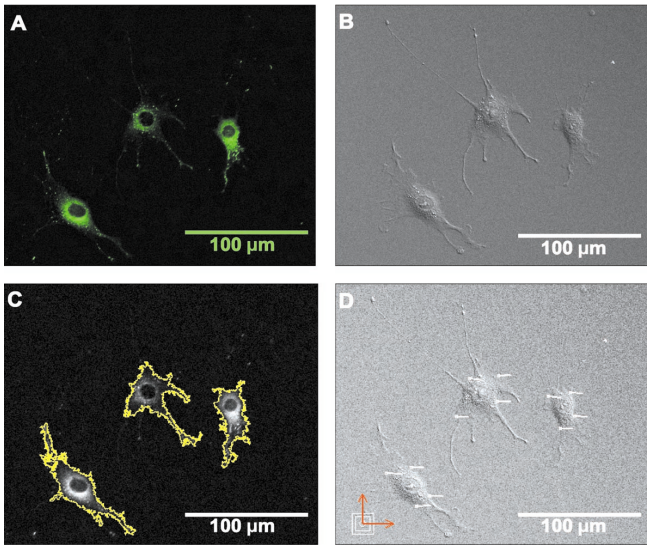

Figure 2. (A) Fluorescence and (B) DIC images of MLO-Y4 cells were captured prior to and immediately following exposure to laminar fluid flow. (C) Changes in intracellular calcium concentrations were calculated by comparing cell ROIs in the fluorescence images before and after flow while (D) digital image correlation was used to determine the strains the cells experienced. The magnification for all images is 200x.

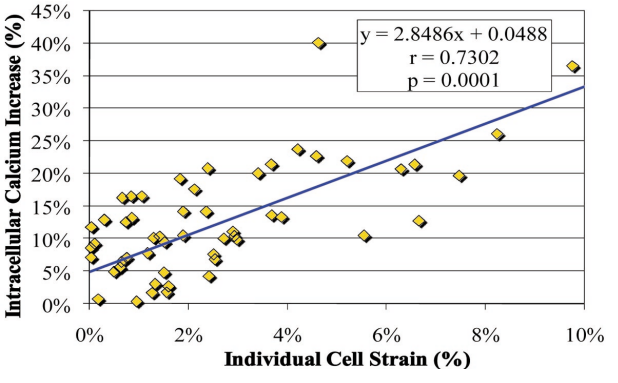

Figure 3. MLO-Y4 osteocyte-like cells show an increase in intracellular calcium concentration levels in response to the cell strain that results from fluid flow induced shear.

Methods: Fluo-4, AM-loaded osteocyte-like MLO-Y4 cells were exposed to uniform laminar fluid flow in a closed system (Figure 1). The upregulation of intracellular calcium was determined from the difference in fluorescence intensity from the cell's basal level prior to exposure to fluid flow and its level immediately following exposure to flow (Figure 2A, C). All fluorescence calculations were conducted on background corrected images. The deformation of each individual osteocyte (n=53) was determined using digital image correlation between images captured prior to and immediately following exposure to fluid flow, and the resulting strains were calculated (Figure 2B, D).

Results: A uniformly applied fluid flow of 8 dynes/cm^2 resulted in measurable strain on MLO-Y4 cells. However, the strain experienced by individual MLO-Y4 cells was not uniform. Measurement of intracellular calcium levels demonstrated that the biologic response elicited by the fluid flow was correlated to the amount of strain each cell experienced (Figure 3). The average strain experienced by the cells was 2.57%±2.28%. The maximum and minimum strains were 9.75% and 0.03%, respectively. The average upregulation of intracellular calcium in the cells was found to be 12.90%±8.26%. The maximum and minimum increases in intracellular calcium were 40.14% and 0.38%, respectively.

Discussion: Osteocytes exposed to uniform laminar fluid flow experienced a range of strains and changes in intracellular calcium levels. Mechanosensing and chemical signaling in osteocytes has been hypothesized to occur at the single cell level, making it imperative to understand the biological responses of individual cells. The work presented here demonstrates that the response of individual osteocytes to a uniform applied fluid flow is variable and well correlated to the amount of strain induced by the fluid flow. This suggests that a range of biological responses is likely to be elicited from mechanically stimulated osteocytes within the same bone as the microstrain experienced by each osteocyte during each loading cycle is likely to be different. Such variability in the mechanostimulation and response of osteocytes would provide bone with a mechanosensitive mechanism for fine local regulation of homeostasis.

References

1. Burger EH, Klein-Nulend J, van der Plas A, Nijweide PJ. Function of osteocytes in bone - their role in mechanotransduction. J Nutr 1995;125(Suppl.7):2020S-3S.
2. Marotti G, Ferretti M, Remaggi F, Palumbo C. Quantitative evaluation on osteocyte canalicular density in human secondary osteons. Bone 1995;16:125-8.
3. Klein-Nulend J, van der Plas A, Semeins CM, Ajubi NE, Frangos JA, Nijweide PJ, Burger EH. Sensitivity of osteocytes to biomechanical stress *in vitro*. FASEB J 1995;9:441-5.
4. Vatsa A, Mizuno D, Smit TH, Schmidt CF, MacKintosh FC, Klein-Nulend J. Bio imaging of intracellular NO production in single bone cells after mechanical stimulation. J Bone Miner Res 2006;21:1722-8.

The authors have no conflict of interest.

P-3

Osteocalcin Is a Stress Hormone Interacting With the Sympathetic Nervous System

P.E. Patterson-Buckendahl[1], J Anyanwu[1], D Kopylov[1], A. Vitenzon[1], A. Shah[1], M. Shahid[1], R. Kvetnansky[2]
[1]Center of Alcohol Studies, Rutgers University, Piscataway, NJ, USA; [2]Institute of Experimental Endocrinology, Slovak Academy of Sciences, Bratislava, Slovakia
E-mail: buckendp@rci.rutgers.edu

Interaction between the sympathetic nervous system (SNS) and bone has received increasing attention in recent years. Adrenergic as well as neuropeptide receptors have been identified on both osteoblasts[1-5] and osteoclasts[6,7]. SNS activation by emotional and physical stressors is also well known, and affects circulating levels of human[8-10], monkey[11] and rodent osteocalcin (pOC)[12-14] in ways that are stressor specific. Most dramatic is the rapid, hormone-like elevation during acute fight/flight response[12]. A target for influence of OC was suggested by immuno-detection of OC in rat dorsal root ganglia (DRG) in cells

of nociceptive and proprioceptive neurons[15-17]. We previously reported altered sensory and stress responses in OC null mutant (KO[18]) mice (ASBMR, 2005). We have extended those observations by subjecting male wildtype (WT) and KO mice to foot restraint immobilization (Immo) for up to 2 hours. Because both native and uncarboxylated OC (uOC) were reported to influence energy metabolism via the pancreas and adipocytes[19], we tested KO mice with and without supplementation with OC or synthetic uOC. We evaluated stress responsive hormones in plasma, adrenal gene expression for enzymes of the catecholamine synthetic pathway and NPY, a neuropeptide decreased by Immo, and localization of OC in DRG. We measured glucose, insulin, adiponectin and leptin in blood taken from 12 KO mice before and 5 and 30 minutes after i.p. injection of saline or 150 ng native mouse OC/g BW (6 each) and immediate Immo. As expected, glucose increased ($p<0.001$) and insulin decreased ($p<0.05$) in all mice. There was a trend for decreased adiponectin and increased leptin, but no effect of OC supplementation, suggesting that stress-induced energy needs over-ride the published effects of OC on this axis. We compared adrenal gene expression for TH, DBH, PNMT in mice Immo for 2 hours and killed immediately (4 per group, KO+OC and WT+saline, compared with 4 KO and 4 WT controls). OC significantly increased TH expression in KO mice after 2 hours Immo compared to KO and WT control and WT Immo. In a second experiment, we subjected WT and KO mice to 2 hours Immo followed by 3 hours recovery. We again measured mRNA for TH, DBH, PNMT as well as NPY in 6 WT and 6 KO unstressed controls compared with 4 groups (6 each: WT and KO injected with saline, KO injected with 300 ng/g BW OC or uOC). Native, fully carboxylated OC significantly increased ($p<0.01$ or less) TH, DBH, and PNMT mRNA in Immo KO compared to both WT and KO controls, whereas it decreased NPY after Immo, consistent with observations in other models. By comparison, uOC administration had lower to non-significant effects. To determine further involvement of SNS, we dissected DRG from unstressed mice perfused with 4% paraformaldehyde. Frozen sections (8 μm) were reacted with goat anti-mouse OC[20] and visualized with FITC conjugated donkey anti-goat serum. Consistent with published reports of OC localization in rat DRG, we observed OC positive staining in wild-type DRG and limb bone. However, we also encountered significant autofluorescence in DRG and brain sections. Therefore, we confirmed the OC localization in DRG by first treating sections with 0.3% hydrogen peroxide in methanol to inactivate native peroxidases and reacting with goat anti-mouse osteocalcin primary antibody followed by horseradish peroxidase conjugated donkey anti-goat secondary antibody and DAB substrate staining. Our data support the hypothesis that fully carboxylated OC has hormonal influence on the adrenal possibly via uptake by DRG innervating the adrenal. Further study of both OC and uOC in stressed and non-stressed animals is warranted.

References

1. Togari A, Arai M, Kondo A. The role of the sympathetic nervous system in controlling bone metabolism. Expert Opin Ther Targets 2005;9:931-40.
2. Takeda S. Central control of bone remodeling. Biochem Biophys Res Commun 2005;328:697-9.
3. Baldock PA, Sainsbury A, Allison S, Lin EJ, Couzens M, Boey D, Enriquez R, During M, Herzog H, Gardiner EM. Hypothalamic control of bone formation: distinct actions of leptin and y2 receptor pathways. J Bone Miner Res 2005;20:1851-7.
4. Baldock PA, Sainsbury A, Couzens M, Enriquez RF, Thomas GP, Gardiner Em, Herzog H. Hypothalamic Y2 receptors regulate bone formation. J Clin Invest 2002;109:915-21.
5. Patel MS, Elefteriou F. The new field of neuroskeletal biology. Calcif Tissue Int 2007;80:337-47.
6. Ishizuka K, Hirukawa K, Nakamura H, Togari A. Inhibitory effect of CGRP on osteoclast formation by mouse bone marrow cells treated with isoproterenol. Neurosci Lett 2005;379:47-51.
7. Takeuchi T, Tsuboi T, Arai M, Togari A. Adrenergic stimulation of osteoclastogenesis mediated by expression of osteoclast differentiation factor in MC3T3-E1 osteoblast-like cells. Biochem Pharmacol 2001;61:579-86.
8. Fujita T, Ohgitani S, Nomura M. Fall of blood ionized calcium on watching a provocative TV program and its prevention by active absorbable algal calcium (AAA Ca). J Bone Miner Metab 1999;17:131-6.
9. Napal J, Amado JA, Riancho JA, Olmos JM, Gonzalez-Macias J. Stress decreases the serum level of osteocalcin. Bone Miner 1993; 21:113-8.
10. Nicholson G, Bryant AE, Macdonald IA, Hall GM. Osteocalcin and the hormonal, inflammatory and metabolic response to major orthopaedic surgery. Anaesthesia 2002;57:319-25.
11. Hotchkiss CE, Brommage R, Du M, Jerome CP. The anesthetic isoflurane decreases ionized calcium and increases parathyroid hormone and osteocalcin in cynomolgus monkeys. Bone 1998;23:479-84.
12. Patterson-Buckendahl P, Kvetnansky R, Fukuhara K, Cizza G, Cann C. Regulation of plasma osteocalcin by corticosterone and norepinephrine during restraint stress. Bone 1995;17:467-72.
13. Patterson-Buckendahl P, Pohorecky LA, Kvetnansky R. Differing effects of acute and chronic stressors on plasma osteocalcin and leptin in rats. Stress 2007;10:163-72.
14. Patterson-Buckendahl PE, Grindeland RE, Shakes DC, Morey-Holton ER, Cann CE. Circulating osteocalcin in rats is inversely responsive to changes in corticosterone. Am J Physiol 1988;254:R828-33.
15. Ichikawa H, Itota T, Torii Y, Inoue K, Sugimoto T. Osteocalcin-immunoreactive primary sensory neurons in the rat spinal and trigeminal nervous systems. Brain Res 1999;838:205-9.
16. Ichikawa H, Jin HW, Fujita M, Nagaoka N, Sugimoto T. Osteocalcin-immunoreactive neurons in the vagal and glossopharyngeal sensory ganglia of the rat. Brain Res 2005;1031:129-33.
17. Ichikawa H, Sugimoto T. The difference of osteocalcin-immunoreactive neurons in the rat dorsal root and trigeminal ganglia: co-expression with nociceptive transducers and central projection. Brain Res 2002;958:459-62.
18. Ducy P, Desbois C, Boyce B, Pinero G, Story B, Dunstan C, Smith E, Bonadio J, Goldstein S, Gundberg C, Brfadley A, Karsenty G. Increased bone formation in osteocalcin-deficient mice. Nature 1996;382:448-52.
19. Lee NK, Sowa H, Hinoi E, Ferron M, AShn JD, Confavreux C, Dacquin R, Mee PF, McKee MD, Jung DY, Zhang Z, Kim JK, Mauvais-Jarvis F, Ducy P, Karsenty G. Endocrine regulation of energy metabolism by the skeleton. Cell 2007;130:456-69.
20. Gundberg CM, Clough ME, Carpenter TO. Development and validation of a radioimmunoassay for mouse osteocalcin: paradoxical response in the Hyp mouse. Endocrinology 1992;130:1909-15.

The authors have no conflict of interest.

P-4

A Novel Role for Collagen *α1* (XI) in Bone Development

K.G. Coonse, R.J. Brown, J.T. Oxford
Boise State University, Department of Biology, Boise, Idaho, USA
E-mail: kcoonse@gmail.com

The fate of mesenchymal-derived osteoprogenitor cells to osteoblasts is dependent on a variety of signaling factors. Among an influential cast of proteins that include growth factors, hormones and transcriptional factors, the alpha 1 chain of collagen type XI (collagen α1(X1)) is a newly described regulator of osteoblast development. The prolonged presence of the globular collagen α1(X1) amino terminal domain (NTD) on the surface of collagen fibrils in the osteoblast matrix suggests this domain may interact with molecules, such as bone morphogenetic proteins (BMPs), to modulate osteogenic cell signaling events. BMPs are extracellular signaling molecules that regulate osteoblast differentiation and function. Suppression of endogenous BMP antagonists, such as noggin, enhances osteoblast mineralization in culture and accelerates *in vivo* bone formation in a mouse model. Recently published, our research demonstrated that inhibition of collagen α1(X1) accelerated mineralization of osteoblasts in culture, while the addition of recombinant collagen α1(X1) NTD inhibited osteoblast mineralization. Further support for a role of collagen XI in osteoblast development is demonstrated by the phenotypic similarities in bone development between the noggin-suppressed mouse and the collagen XI-suppressed chondrodystrophic mouse. These findings support a role for collagen α1(X1) as a mediator of osteogenic signaling, and lead us to investigate the hypothesis that collagen α1(X1) mediates osteoblast development via interaction with BMP cell signaling. To test this hypothesis, C2C12 osteoprogenitor cells under the influence of BMP-2 were observed in the presence or absence of collagen α1(XI). Activation of BMP-responsive

Smad proteins was observed by confocal microscopy and expression of osteoblast-specific markers of differentiation were evaluated. This work identifies a second function of collagen α1(XI) in bone formation that is separate from its well established role in limiting collagen fibril diameter. In addition to providing a more thorough understanding of the mechanisms that regulate osteoblast development, this knowledge may potentially enhance development of novel therapeutic agents for the treatment of bone disease.

The authors have no conflict of interest.

P-5

Gymnastic Loading and Distal Radius Cross-sectional Asymmetry

J.N. Dowthwaite, R.M. Hickman, J.A. Spadaro, T.A. Scerpella
Department of Orthopedic Surgery, SUNY Upstate Medical University, Syracuse, NY, USA
Email: dowthwaj@upstate.edu

Mechanical loading during human growth generates adaptations in areal bone mineral density; these adaptations appear to occur via enlarged total bone and cortical dimensions, elevating theoretical bone strength[1]. It is unknown whether human bone adapts to mechanical loading in a symmetrical manner. The non-dominant radius serves as a specific barometer of weight-bearing impact loading via artistic gymnastics participation and is a suitable site for pQCT evaluation of bone architecture[1]. Therefore, we evaluated the non-dominant radius in post-menarcheal ex-gymnasts/gymnasts and non-gymnasts, hypothesizing that the radius adapts asymmetrically to gymnastic loading during growth, with greater periosteal expansion in the medial-lateral plane than the antero-posterior plane. To test this hypothesis, we used pQCT to measure aspect ratios and bone widths from a cross-section of the radial diaphysis (33% region of interest, X plane=medial-lateral, Y plane=anteroposterior), comparing output for post-menarcheal non-gymnasts versus girls exposed to gymnastic loading during growth.

Subjects from an ongoing longitudinal study of gymnastics-related bone accrual were recruited for pQCT scans of the distal radius. Scans of the 33% site[2] (Stratec XCT 2000) were performed on 48 post-menarcheal girls classed as ex/gymnasts (n=27, current or ex-gymnasts) or non-gymnasts (n=21) based on childhood "gymnastic exposure". "Gymnastic exposure" was defined as years with gymnastic participation of at least 5 h/wk. Maximum X (medial-lateral) and Y (anteroposterior) plane bone widths were measured using the XCT 2000 ruler function. Aspect ratios were calculated (X-plane width, numerator; Y-plane width, denominator). Height was measured using wall-mounted rulers. ANOVA compared aspect ratios for ex/gymnasts versus non-gymnasts. ANCOVA compared X and Y plane widths, adjusting for gynecological age and height. Means, standard errors and significance (alpha=0.05) are reported.

Subjects averaged 17.0 years old (gynecological age 3.9 years) and 162.0 cm tall. Ex/gymnasts and non-gymnasts did not differ in chronological age, gynecological age, total body FFM, BMI, percent body fat and calcium intake; mean height (ex-gym=159.9 cm+7.4; non=163.0 cm+7.3) and gymnastic exposure differed (ANOVA $p<0.05$). For ex/gymnasts, "gymnastic exposure" ranged from 1 to 11 yrs; mean participation over the "gymnastic exposure" period ranged from 5-18.4 h/wk. Ex/gymnasts exhibited 14% higher adjusted X-axis diameters than non-gymnasts (ex/gymnasts =14.6 mm; non-gymnasts=12.8 mm (ANCOVA $p<0.001$)). Ex/gymnasts also exhibited an 11% advantage over non-gymnasts for Y-axis diameter (ex/gymnasts=12.1 mm; non-gymnasts=10.9 mm (ANCOVA $p<0.001$). The 3% ex/gymnast versus non-gymnast aspect ratio difference was not statistically significant (ex/gymnasts=1.21; non-gymnasts=1.17 (ANOVA $p=0.10$).

Weight-bearing impact loading during growth appears to expand both medial-lateral and antero-posterior periosteal dimensions. Aspect ratios suggest loading-induced asymmetry; however, differences did not achieve statistical significance in this limited sample.

References

1. Dowthwaite JN, Flowers PPE, Spadaro JA, Scerpella TA. Bone geometry, density and strength indices of the distal radius reflect loading via childhood gymnastic activity. J Clin Densitom 2007;10:65-75.
2. Dowthwaite JN, Hickman RM, Kanaley JA, Ploutz-Snyder RJ, Spadaro JA, Scerpella TA. Distal radius strength: a comparison of DXA-derived vs. pQCT-measured parameters in adolescent females. J Clin Densitom 2008;(in press). DOI:10.1016/j.jocd.2008.06.001

All authors have no conflict of interest.

P-6

A Novel Deletion in DMP1 is Associated with a Severe ARHR Phenotype: A New Contiguous Gene Syndrome?

*E.G. Farrow[1], S.I. Davis[1], L.M. Ward[2], L.J. Summers[1], J.S. Bubbear[3], R. Keen[3], T.C.B. Stamp[3,4], L.R.I. Baker[5], K.E. White[1]
[1]Indiana University School of Medicine, Indianapolis, IN; [2]Children's Hospital of Eastern Ontario, and the University of Ottawa, Ottawa, Ontario, Canada; [3]Royal National Orthopaedic Hospital, Stanmore, Middlesex, UK; [4]UCL Hospital, London UK; [5]Department of Nephrology, St. Bartholomews and Royal London Hospitals, London UK
E-mail: efarrow@iupui.edu

Recent findings support a critical role for the osteocyte as a key cell in the bone-kidney endocrine axis of phosphate metabolism. Autosomal recessive hypophosphatemic rickets (ARHR), characterized by isolated renal phosphate wasting, rickets, and elevated serum fibroblast growth factor-23 (FGF23), is caused by mutations in the osteocyte-specific gene Dentin matrix protein-1 (*DMP1*), a member of the SIBLING protein family. To further understand the role of *DMP1* in ARHR, we examined a kindred with a severe clinical phenotype consisting of marked hypophosphatemia, persistent osteomalacia upon bone biopsy, increased bone density, stunted growth, nerve deafness, facial and dental abnormalities, and learning disabilities. The affected siblings (brother and sister) had significantly elevated serum FGF23 levels at 91.5 and 199 pg/mL (normal 10-54), whereas the unaffected father was normal (42 pg/ml). Mutational analysis revealed normal PCR amplification and sequences for the exons comprising *DMP1* in the father, however in the affected individuals, there was complete absence of *DMP1* exons 3 through 6 as well as an intronic DNA sequence 50 kb telomeric to DMP1. The integrin-binding sialoprotein (IBSP) locus is telomeric to *DMP1* on chromosome 4q21-25, and exon 1 of IBSP was intact in the affected individuals and in the father. Therefore, these patients have a deletion in *DMP1* of at least 50 kb, and maximally 150 kb, potentially representing a new contiguous gene syndrome. In summary, we have identified a novel deletion in *DMP1* associated with elevated FGF23 and severe ARHR, further expanding the genetic spectrum of alterations that cause this disorder.

The author has no conflict of interest.

P-7

Non-invasive (pQCT) Analysis of the Metabolic Impact of Chronic Haemodialysis (CHD) on Bone Biomechanics and Muscle-Bone Interactions in Bearing and non-bearing Limbs of Men and Women

J.L. Ferretti, S. Feldman, I. Grappiolo, R. Capozza, G. Cointry, G. Inchauspe, B. Radice, P. Reina, P. Castellini, G. Nicola, F. Acosta
Center of P-Ca Metabolism Studies (CEMFoC) and Service of Dialysis and Transplantation; Faculty of Medicine/University Hospital, National University of Rosario, Argentina
E-mail: jlferretti@arnet.com.ar

Aim and methods: The aim of this investigation was to describe the metabolic impact of CHD on the musculoskeletal system in men and women, as described by tomographic indicators, and following biomechanical criteria.

With that purpose, the following pQCT indicators (XCT-2000, Stratec, 0.5 mm voxel size, 710 mg.cm^{-1} threshold for cortical bone detection) were determined in tibial (4, 14, 38, and 66% sites) and radial (4 and 66% sites) scans of 21 men and 14 women aged 15-66 years undergoing CHD:

- Bone mass indicators:
  - Trabecular and cortical BMC (TbC, CtC) (tibial/radial 4% sites, 45% concentric peeling)

- Trabecular vBMD (TbD) (tibial/radial 4% sites, 45% concentric peeling)
- Cortical CSA (CtA) (radial 66% site, tibial 38% site)
- Trabecular/cortical mass relationship (tibial ToC 4% vs 14% or 38% sites)

- Bone tissue mineralization indicator (radial 66% site, tibial 38% site):
  - Cortical vBMD, corrected from the partial-volume effect (CtD)
- Diaphyseal design indicators (radial 66% site, tibial 38% site):
  - Endosteal perimeter (EoPm)
  - Cortical thickness (CtTh)
  - Bending and torsion moments of inertia (CSMI's)
- Diaphyseal strength indicators (radial 66% site, tibial 38% site):
  -Bone Strength Indices (x,y,pBSI's)
  -Stress-Strain Index (pSSI)
- Muscle strength indicators (66% sites):
  -Height-adjusted muscle CSA (mCSA).

Z-scores of these data were calculated with reference to those obtained the same way in 260 healthy adults (60 men, 80 pre-MP women, 120 post-MP women) of comparable age.

The natural, hyperbolic relationships observed between CSMIs (diaphyseal design indicators, y) and CtD (material "quality" indicator, x), which we have called "distribution/quality" (d/q) curves, were regarded as descriptive of the ability of the bone *mechanostat* to re-distribute the compacta in the cortices as a function of its intrinsic stiffness. Relationships between bone mass, design and strength indicators with mCSA were analyzed in order to assess the muscle-bone interactions in these patients.

The pQCT data were also correlated with serum PTH activity and time on dialysis to assess the impact of the metabolic disturbance on the above indicators and relationships.

Results: Both CHD men and women showed significant impairments of TbC, TbD, and trabecular/cortical relationship, and comparatively less intense reductions of CtC, CtA, BSIs and SSI with respect to their specific controls. Bone mass loss was generally greater in women than men, and in lower than upper limbs.

No changes were induced in CtD.

EoPm was generally increased, and CtTh consecuently reduced. A relatively mild impairment in CSMIs was observed, only significant in women.

The d/q curves showed significantly lower ordinates than those observed in controls only in the CHD women.

The mCSA was generally reduced, especially in the women.

Bone mass (but not CSMIs, BSIs, or SSI) per unit of mCSA decayed more severely in women than men.

In general terms, the described affectation of bone indicators and the biomechanical changes in bone-muscle interactions were more evident or significant in tibial than in radial scans.

All the described changes correlated significantly with both serum PTH and time on dialysis.

Interpretation: The CHD-induced osteopenia was more significantly affected with respect to healthy controls in metaphyseal regions with thin cortices than in diaphyses, and predominantly so in the women.

The cortical loss seemed to have resulted predominantly from endosteal resorption (larger EoPm) rather than from an enhanced intracortical remodeling (little CHD impact on CtD). The comparatively milder CHD impact on CtD described in our patients as compared with that reported by other investigators may derive from the PVE-adjustment applied to the vBMD data in this study. This suggests that the cortical thinning should be taken into account as a potential source of technical errors for cortical vBMD data in these cases. In agreement with others, we have observed that this adjustment seems to become critical when CtTh was lower than 2 mm in our patients.

The moderate cortical thinning resulting from that effect had a relatively low impact on the CSMIs. The mechanical orientation of bone modeling by bone *mechanostat* as a function of mechanical usage (d/q curves, CSMI/CtD ratio) was little affected by CHD and only in women, suggesting a metabolic (not mechanical) disturbance.

Bone loss was associated to PTH activity and time on dialysis in all patients, also suggesting a metabolic disturbance.

Predominance of effects in the legs may be associated with some neuromuscular, stroll-related (i.e., mechanical, not metabolic) problems, which are currently being more deeply investigated.

The authors have no conflict of interest.

P-8

Differential Effects of Diabetes on the Cortical vs. Trabecular Bone Compartments in Two Inbred Mouse Strains

J. Fowlkes[1], J. Nyman[2], C. Bunn[1], G. Cockrell[1], E. Wahl[1], C. Lumpkin[1], K. Thrailkill[1]
[1]University of Arkansas for Medical Sciences, Little Rock, AR, USA; [2]Vanderbilt Center for Bone Biology, Nashville, TN, USA
E-mail: fowlkesjohnl@uams.edu

We have previously demonstrated marked inhibition of intramembraneous bone formation in diabetic mice, by using a model of tibial distraction osteogenesis paired with short-term diabetes (~3 weeks duration). The objective of the present study was to examine the effects of more prolonged diabetes on bone phenotype in two inbred mouse strains, which differ in their inherent susceptibility to diabetic co-morbidity (i.e., C57BL6 mice vs. DBA2J mice). Male mice of each strain±treatment with streptozotocin (STZ: 40 mg/kg/day x 5 days at 11 weeks of age, to induce diabetes) were provided free access to food and water and monitored weekly for glucosuria and weight change over 14 weeks. At sacrifice, serum concentrations of glucose, fructosamine, osteocalcin, PINP and mTRAP were measured and the right femur was harvested and analyzed by μCT and biomechanical testing.

We observed phenotypic differences in the femur mid-shaft between control C57BL6 and DBA2J mice at 25 weeks of age. Specifically, the periosteal size of the femur mid-shaft was smaller in DBA2J mice than C57BL6 mice, but the bone volume of the diaphysis was not different between the two strains. Therefore, the cortices of the DBA2J femur were significantly thicker than the C57BL6 femur ($p<0.001$). The DBA2J femur mid-shaft also had greater volumetric BMD ($p<0.001$); consequently, the femur of the DBA2J mouse was considerably stronger than the femur of C57BL6 mice. In contrast to the bone volume in the femur mid-shaft, the volume of trabecular bone in the metaphysis was greater in the C57BL6 mice than in DBA2J mice ($p<0.001$). This higher BV/TV was due to a higher number of trabeculae (Tb.N) and thicker trabeculae (Tb.Th) in the C57BL6 bone, compared with the DBA2J bone ($p<0.001$ for both). Both C57BL6 and DBA2J mice treated with STZ, compared with their respective control groups, exhibited: 1) glucosuria from weeks 4-14; 2) significantly elevated serum glucose (C57BL6: 422.4±131.9 mg/dl vs. 138.2±46.7, $p<0.001$; DBA2J: 497.0±206.0 vs. 173.0±84.3, $p<0.01$) and fructosamine (C57BL6: 418.8±24.2 μmole/L vs. 250.2±21.6; DBA2J: 396.5±22.8 vs. 238.2±20.8, $p<0.001$ for both); and 3) lower body weight ($p<0.01$) at 14 weeks, thus confirming a 10-week duration of diabetes. With STZ-induced diabetes in C57BL6 and DBA2J mice, there were significant changes in the 3-D structure of the bone (Table). Diabetes

Skeletal phenotype (ME.AN±SD)	C57Bl/6 Control (n=6)	C57Bl/6+ STZ (n=5)	*p*-value	DBA/2J Control (n=6)	DBA/2J+ STZ (n=4)	*p*-value
Total volume (mm^3)	2.41±0.25	2.15±0.13	=0.06	1.52±0.13	1.29±0.07	=0.01
Bone volume (mm^3)	1.04±0.1	0.86±0.09	=0.01	0.97±0.08	0.68±0.05	<0.001
Cortical thickness (mm)	0.18±0.01	0.16±0.01	<0.01	0.24±0.01	0.17±0.01	<0.001
BMD (mg/cm^3)	1444±19	1443±12	NS	1575±7	1524±14	<0.001
Yield force (N)	10.09±1.80	8.51±1.37	NS	18.58±1.75	9.44±2.20	<0.001
Yield strength (MPa)	85.76±18.64	88.79±15.09	NS	240.42±14.00	176.86±47.32	=0.01
BV/TV	0.19±0.05	0.11±0.02	<0.01	0.08±0.01	0.05±0.02	=0.02
Tb.N	4.69±0.43	4.06±0.15	=0.01	3.43±0.45	3.40±0.39	NS
Tb.Th	0.055±0.004	0.046±0.002	=0.001	0.047±0.002	0.035±0.005	<0.001
Tb.Sp	0.20±0.02	0.24±0.01	<0.01	0.30±0.05	0.30±0.04	NS
Serum osteocalcin	55.5±12.6	15.8±8.5	<0.001	33.4±34.1	10.4±5.1	NS
Serum PINP	13.5±4.5	17.2±3.1	NS	18.2±7.9	19.0±3.7	NS
Serum mTRAP	4.0±0.8	8.0±2.1	<0.01	4.1±3.4	5.7±2.1	NS

caused a thinning of the cortices, and this effect was more severe in the DBA2J mice. The diabetic state also decreased the BMD of the femur mid-shaft, but only in the DBA2J mice. Therefore, diabetes mildly affected the structural strength (i.e., yield force) of the C57BL6 femur mid-shaft, whereas diabetes severely affected both structural strength and material strength of the DBA2J femur mid-shaft. The diabetic state also caused a decrease in trabecular bone volume in the metaphysis of both mouse strains, but this effect was more pronounced in the C57BL6 mice than in the DBA2J mice. In the C57BL6 strain, the loss in BV/TV was due to both a decrease in Tb.N and Tb.Th. In the DBA2J strain, the loss was mainly due to a decrease in Tb.Th, whereas diabetes had no effect on Tb.N or trabecular spacing (Tb.Sp). Coincident with these changes in bone phenotype, in diabetic C57BL6 mice, serum concentrations of osteocalcin were decreased while mTRAP concentrations were increased. In diabetic DBA2J mice, similar though modest and statistically insignificant changes in serum bone marker concentrations were observed. In conclusion, we have demonstrated significant differences between two inbred mouse strains, with and without 10 weeks of diabetes, in the cortical vs. the trabecular bone phenotype. Explanations for these differences have not been delineated, but could reflect underlying differences in the genetic background or body composition of these two strains, or could be a manifestation of concurrent diabetic nephropathy (albuminuria), which develops in diabetic DBA2J mice.

The authors have no conflict of interest.

P-9

Non-resorbing Osteoclasts Secrete Anabolic Factors Activating Bone Formation *In Vitro* and *In Vivo*

*K. Henriksen[1], A.V. Neutzsky-Wulff[1], C. Christiansen[1], K.D. Hausler[2], M. Ciccomancini[2], C. Christiansen[2], M. Gillespie[2], T.J. Martin[2], M.A. Karsdal[1]
[1]Nordic Bioscience A/S, Herlev, Denmark; [2]St. Vincent's Institute of Medical Research, Melbourne, Australia
E-mail: kh@nordicbioscience.com

Human osteopetrotic mutations leading to defective acidification of the resorption lacuna, such as mutations in the a3 subunit of the V-ATPase or the chloride channel ClC-7, lead to low bone resorption, increased numbers of osteoclasts and increased bone formation. Findings indicating that the osteoclasts, independent of resorption, are sources of anabolic signals for the osteoblasts.

To clarify the apparent imbalance between osteoclast and osteoblast activity we investigated the osteopetrotic phenotype of ClC-7 deficient mice with respect to osteoclast numbers, bone resorption, and bone formation *in vivo* and *in vitro*. We collected conditioned media from resorbing and non-resorbing osteoclasts, and investigated their activities in bone formation assays and reporter systems sensitive to a panel of anabolic stimuli for osteoblasts.

ClC-7 KO mice and their wildtype (WT) littermates were sacrificed at 4-5 weeks of age. Biochemical markers of resorption (CTX-I), osteoclast number (TRACP 5b), and osteoblast activity (ALP) were measured in serum. Histological examination of bone formation and osteoclast number was performed. Splenocytes were used to evaluate osteoclastogenesis and resorption measured by CTX-I, Ca^{2+}, and TRACP. Osteoblastogenesis *in vitro* was investigated using calvarial osteoblasts, and nodule formation was examined by alizarin red.

Conditioned media from human osteoclasts cultured on either bone slices or plastic were collected. Conditioned media were applied to cultures of MC3T3-E1 pre-osteoblasts, followed by bone formation assessment by Alizarin red and Von Kossa staining after 20 days' culture. We assessed key osteoblast regulatory pathways by using UMR106.01 cells transiently transfected with several reporter constructs. These were the TCF/LEF reporter, the OSE reporter, NFAT, AP-1 and NFkB.

Serum markers showed reduced resorption per osteoclast, but increased osteoclast numbers and increased osteoblast activity. High numbers of osteoclasts and ongoing bone formation was observed in bone sections. *In vitro* osteoclastogenesis of the ClC-7 -/- osteoclasts was normal, although the osteoclasts were non-resorbing. Bone formation by ClC-7 -/- calvarial osteoblasts was normal.

Conditioned media from osteoclasts cultured on bone or plastic stimulated nodule formation by the MC3T3-E1 cells to levels comparable to stimulation with 10ng/mL BMP-2. Conditioned media from osteoclasts cultured on both bone and plastic specifically induced activation of the TCF/LEF response system at a level comparable to induction by 20 ng/mL of Wnt3A. The conditioned medium signals were inhibited, albeit to different extents, by addition of either 100ng/mL of DKK1 or 1 μg/mL of sclerostin.

In summary, we present evidence that the uncoupling phenotype seen in the ClC-7 deficient mice is caused by defective resorption leading to increased osteoclast numbers, which then produce anabolic factors leading to activation of the osteoblasts and thereby bone formation. Furthermore, we present evidence that osteoclasts secrete an activity that stimulates osteoblastic bone formation via the canonical want cascade.

The authors have no conflict of interest.

P-10

BMP3-Null Aged Mice Display Increased Trabecular Bone Volume and Reduced Cross-Sectional Area at the Mid-Femoral Diaphysis

L. Huang[1], R. Raz[1], D.A. Panus[2], Y. Xue[1], D.M. Valenzuela[1], G.D. Yancopoulos[1], A. Murphy[1], M. Bouxsein[2], V. Rosen[3], A.N. Economides[1]
[1]Regeneron Pharmaceuticals, Inc., Tarrytown, NY, USA; [2]Beth Israel Deaconess Medical Center, Boston, MA, USA; [3]Harvard School of Dental Medicine, Boston, MA, USA
E-mail: lily.huang@regeneron.com

BMP3 was originally purified from bovine bone matrix as osteogenin, an activity with osteogenic function. However, it has later been identified as an inhibitor of osteogenic BMPs and a negative regulator of bone density in mice. Using VelociGene® technology, we have generated BMP3 homozygous-null (KO) mice where the first exon (encoding the N-terminal part of the precursor region) was replaced in frame with the LacZ reporter. We used micro-computed tomography to evaluate trabecular bone microarchitecture in the distal femur and the vertebral body, as well as cortical bone morphology in the mid-femoral diaphysis. We found that in aged animals (36 to 44 weeks), trabecular bone volume in the distal femur and vertebral body was significantly higher in KO compared to wild type littermate controls (30% to 70%) primarily due to increased trabecular number. At the mid-femoral diaphysis, the relative cortical bone area fraction and cortical thickness was unchanged, but the total cross-sectional area, bone area and medullary area were smaller in KO than in controls, correlating with a reduction in body weight. The results of this study indicate that loss of BMP3 has a protective role against age-related bone loss and uncover a role for BMP3 in the regulation of body mass.

The authors have no conflict of interest.

P-11

Ablation of the GALNT3 Gene in Mice Leads to Low Circulating FGF23 Concentrations and Hyperphosphatemia Despite Increased FGF23 Gene Expression

*S. Ichikawa[1], A.H. Sorenson[1], T.A. Fritz[2], A. Moh[4], D.S. Mackenzie[1], S.L. Hui[1], M.J. Econs[1,3]
[1]Department of Medicine, Indiana University School of Medicine, Indianapolis, IN, USA; [2]Section on Biological Chemistry, NIDDK, National Institutes of Health, Bethesda, MD, USA; [3]Department of Medical and Molecular Genetics, Indiana University School of Medicine, Indianapolis, IN, USA; [4]Deparment of Microbiology and Immunology, Indiana University School of Medicine, Indianapolis, IN, USA
E-mail: ichikawa@iupui.edu

Familial tumoral calcinosis is characterized by ectopic calcifications and hyperphosphatemia. Three genes associated with this disease are fibroblast growth factor 23 (FGF23), Klotho (KL), and UDP-N-acetyl-alpha-D-galactosamine: polypeptide N-acetylgalactosaminyltransferase 3 (GALNT3). GALNT3 encodes an enzyme that O-glycosylates FGF23 in a furin-like convertase recognition sequence, thereby preventing proteolytic processing of FGF23 and allowing secretion of intact FGF23. Ablation of FGF23 and KL in mice results in severe hyperphosphatemia as well as vascular and soft-tissue calcifications. In this study, we generated mice deficient in GALNT3. Mice with a homozygous deletion of GALNT3 were hyperphosphatemic as seen in patients with tumoral calcinosis. GALNT3-deficient mice also exhibited inappropriately normal 1,25-dihydroxyvitamin D [$1,25(OH)_2D$] levels and

decreased alkaline phosphatase activity. In response to hyperphosphatemia, GALNT3-deficient mice had significantly increased FGF23 expression in the bone, but decreased circulating intact FGF23 levels, compared to wild-type and heterozygous mice. Renal expression of sodium-phosphate co-transporter IIa and KL were also elevated in GALNT3-deficient mice. However, histological and radiographic analyses of homozygous mice revealed no apparent calcifications or abnormalities in the tissues evaluated. Interestingly, GALNT3-deficient males, but not females, showed growth retardation, infertility, and significantly increased bone mineral density (BMD). In summary, ablation of GALNT3 enhanced expression of the FGF23 gene, but impaired secretion of FGF23, leading to decreased circulating FGF23 and hyperphosphatemia. Our findings provide the evidence that GALNT3 plays an essential role in proper secretion of FGF23 in mice.

The authors have no conflict of interest.

P-12

Effects of Vitamin K2 and Risedronate on Bone Formation and Resorption, Osteocyte Lacunar System and Porosity in the Cortical Bone of Glucocorticoid-Treated Rats

J. Iwamoto[1], H. Matsumoto[1], X. Liu[2], J.K. Yeh[2]
[1]Department of Sports Medicine, Keio University School of Medicine, Shinjuku-ku, Tokyo, Japan; [2]Metabolism Laboratory, Department of Medicine, Winthrop-University Hospital, NY, USA
E-mail: jiwamoto@sonata.okaka.or.jp

The purpose of the present study was to examine the effects of vitamin K2 and risedronate on bone formation and resorption, the osteocyte lacunar system and porosity in the cortical bone of glucocorticoid (GC)-treated rats. Forty-nine female Sprague-Dawley rats, 3 months of age, were randomized into five groups according to the following treatment schedule: age-matched control, GC administration, and GC administration with concomitant administration of vitamin K2, risedronate, or vitamin K2+risedronate. At the end of the 8-week experiment, classical bone histomorphometric analysis was performed and the osteocyte lacunar system and porosity were evaluated on the cortical bone of the tibial diaphysis. GC administration decreased percentage cortical bone area and increased percentage marrow area as a result of decreased periosteal bone formation and increased endocortical bone erosion, and increased cortical porosity. Vitamin K2 prevented a reduction in periosteal bone formation, but did not affect percentage cortical bone and marrow areas. Risedronate prevented a reduction in periosteal bone formation and an increase in endocortical bone erosion, resulting in prevention of alterations in percentage cortical bone and marrow areas. Both vitamin K2 and risedronate increased osteocyte density and lacunar occupancy, and prevented a GC-induced increase in cortical porosity. Vitamin K2 and risedronate had additive effects on osteocyte density and lacunar occupancy and a synergistic effect on cortical porosity. The present study showed the efficacy of vitamin K2 and risedronate for bone formation and resorption, the osteocyte lacunar system and porosity in the cortical bone of GC-treated rats.

The authors have no conflict of interest.

P-13

Hydroxyapatite Scaffolds with Multi-Scale Porosity

A.J. Wagoner Johnson
Department of Mechanical Science and Engineering, Bioengineering, and the Institute for Genomic Biology, University of Illinois at Urbana-Champaign, IL, USA
Email: ajwj@illinois.edu

Hydroxyapatite (HA) has long been recognized as a promising synthetic bone substitute material; the structure and composition are similar to the mineral phase of bone and it is biocompatible, bioactive, and osteoconductive. However, clinical applications for HA have been limited because of its inherent brittle behavior and low strength in porous form, the form required for integration into host bone.

Pore size, volume, and interconnectivity have been shown to be highly influential for bone ingrowth and have been studied in some detail, but the optimal combination is still debated. There is, however, general agreement among researchers that pore sizes or connections that are 100 μm or greater must be present to allow osteogenic cells and vasculature to penetrate the scaffold and for tissue to mineralize[1,2]. Osteoid and fibrous tissue ingrowth has been observed in scaffolds with interconnection sizes greater than 40 mm and 5 mm, respectively[3]. Our previous work[4] and the work presented, along with the work of others[5], has shown that HA scaffolds containing both macroporosity (defined by some as >50 μm) and microporosity (<10 μm), referred to as multi-scale porosity here, may further promote bone ingrowth.

The results from two sequential *in vivo* studies in pigs investigating the effects of multi-scale porosity are summarized. Two types of scaffolds were compared and each consisted of alternating layers of orthogonal HA rods with center-to-center spacing of 720 μm in-plane and 585 μm out-of-plane, which resulted in a lattice-like structure with macropore sizes ranging between approximately 200 μm and 875 μm. One type of scaffold consisted of solid rods, referred to here as non-microporous (NMP) scaffolds. The scaffolds with multi-scale porosity consisted of rods containing interconnected micropores 5-8 μm in diameter, referred to here as microporous (MP) scaffolds. In the original pilot study MP and NMP scaffolds were doped with BMP-2 and implanted in muscle for 8 weeks[1], and in the second study MP and NMP scaffolds without BMP-2 were implanted in bone for 3, 6, 12, and 24 weeks (data for 3 weeks is described here).

The intramuscular study showed bone growth exclusively in MP scaffolds, but not in NMP scaffolds. Further, bone appeared to grow into the micropores, despite previous reports that this is not possible for pores of this size. The study could not prove whether the bone formation resulted from the presence of the microporosity or from the interaction of the BMP-2 with the microporosity, nor could the study determine whether bone had grown into the micropores because the stain used (Toluidine Blue) does not distinctively and differentially stain mineralized and unmineralized tissue. The subsequent study in which samples were implanted into the mandibles of pigs showed that the total bone volume and bone penetration into the scaffolds was greater for MP scaffolds as compared to NMP scaffolds. The study also demonstrated that the improvement of bone growth in MP scaffolds resulted from the microporosity and not the BMP-2/micropore interaction. Finally, the study confirmed that bone did indeed grow into the micropores by using Sanderson's rapid bone stain with acid fuchsin counterstain, which stains unmineralized tissue blue and mineralized tissue red, respectively.

We hypothesize that the interconnected microporosity can offer an additional length scale for tissue growth. Bone formation at multiple lengthscales will create a co-continuous composite structure, in which both phases (bone and HA) are continuous throughout the entire structure on both the macro- and micro- length scales. Such a composite could result in significantly improved *in vivo* properties, such as toughness, and extend the clinical use of HA scaffolds to large and load-bearing defects. This, in turn, could improve the quality of life for millions who would receive bone grafts or for whom grafts have been unsuccessful, and significantly decrease health care costs associated with graft procedures.

Acknowledgements

The author acknowledges the financial support of the Aircast Foundation and the NSF (0414956), and the Sun Valley Workshop for the Alice L. Jee Memorial Young Investigator Award. The author also acknowledges the technical contributions from collaborators M. B. Wheeler, S. G. Clark, and students S. K. Lan, S. Polak, J. Cordell, S. Wilson, A. Maki, and M. Poellmann at the University of Illinois.

References

1. Hing K. Bioceramic bone graft substitutes: influence of porosity and chemistry. Int J Appl Ceram Technol 2005;2:184-99.
2. Karageorgiou V, Kaplan D. Porosity of 3D biornaterial scaffolds and osteogenesis. Biomaterials 2005;26:5474-91.
3. Klawitter J, Hulbert S. Applications of porous ceramics for the attachment of load bearing orthopaedic applications. J Biomed Mater Res Symp 1971;2:161-229.
4. Woodard J, Hilldore A, Lan S, Park CJ, Morgan A, Eurell J, Clark S, Wheeler M, Jamison R, Wagoner Johnson A. The mechanical properties and osteoconductivity of hydroxyapatite bone scaffolds with multi-scale porosity. Biomater 2007;28:45-54.

5. Hing K, Annaz B, Saeed S, Revell P, Buckland T. Microporosity enhances bioactivity of synthetic bone graft substitutes. J Mater Sci Mater Med 2005;16:467-75.

The author has no conflict of interest.

P-14

Morphological Study of Retinoic Acid-induced Malformation of Skeletal Tissues During Axolotl Limb Regeneration

*B. Li[1], N. Rao[1], A. Robling[2], F. Song[1], J. Li[1], D. Stocum[1]
[1]Department of Biology, School of Sciences; [2]Department of Anatomy and Cell Biology, School of Medicine, Indiana University-Purdue University, Indianapolis, IN, USA
E-mail: eli79@iupui.edu

Axolotls (*Ambystoma mexicanum*) are able to regenerate a perfect replica of a missing limb regardless of amputation level. Two critical events are involved in the epimorphic regeneration of an amputated axolotl limb: blastema formation and the re-differentiation of stem-like blastema cells into complex limb tissues (cartilage, bone, muscle, etc.). Methylene blue staining of cartilage has shown that all-trans retinoic acid (RA) administrated at the early stages of limb regeneration can proximalize regenerated skeletal elements. In this study, X-ray radiography and micro-computed tomography (micro-CT) were used for the first time to image the RA-induced malformation of mineralized bones during the forelimb regeneration of adult axolotls. On day 9 post-amputation (through distal radius-ulna), porous poly(lactic-co-glycolic acid) (PLGA) scaffolds incorporated with RA were implanted in dorsal fin tunnel for the sustained-delivery of RA over the time course of limb regeneration. Following blood vessel formation around the implants, the implants were integrated with surrounding tissue, which ensured the release of RA into the bloodstream. On day 45 post-implantation, for both control and RA-treated groups, X-ray radiographs showed the regenerating radius and ulna with lower bone mineral density. Meanwhile, the periphery of pre-existing bone matrix proximal to amputation plane was resorbed by osteoclasts and replaced by newly deposited bone matrix through an endochondral ossification process. For the RA-treated group, the regenerated radius and ulna merged at the distal end and a shoulder girdle protruded from the posterior ulna toward the ventral direction, indicating the regenerating bone elements undergoing proximal-distal duplication, which was further confirmed by micro-CT and histology studies.

The authors have no conflict of interest.

P-15

Does Oxygen Tension Determine the Metabolic Responses of Osteocytes to Fluid Shear Stress?

D. Liu
Department of Developmental Sciences/Orthodontics, Marquette University School of Dentistry, Milwaukee, WI, USA
E-mail: dawei.liu@marquette.edu

Osteocytes have been found to be functioning as mechanosensors responding to fluid shear stress generated in the lacunae-canaliculi system under mechanical loading. Oxygen tension is critical to cellular functions, which is a function of perfusion (fluid shear) rate of interstitial fluid. When bone is mechanically challenged, the osteocytes *in situ* are influenced by the fluid shear and its associated oxygen tension. However, whether these two factors interact with each other in causing the metabolic changes of osteocytes is not known. We hypothesize that fluid shear-induced metabolic changes of osteocytes is independent of oxygen tension. To testify this, MLO-Y4 osteocytes were seeded on a Ø60mm tissue culture dish and grown in α-MEM with 5% FBS and 5% CS. Upon 80% confluent, the cells were serum starved and simultaneously subjected to 1% hypoxic challenge using a commercially available hypoxia chamber (Billups-Rothenberg, Inc., CA, USA) for 12 hours, while the controls were kept under 95% air and 5% CO_2. After 12 hours of starvation and hypoxic challenge, the hypoxic chamber with the cells in it was rocked on a rocking plate at 0.1Hz in a 37°C thermo box. Thirty minutes after rocking, half of the dishes were taken out of the chamber and the cells were lysed for detecting activation of MAPK (ERK1/2). To examine metabolic changes, the cells were subjected to rocking for 1 hour followed by 6 hours of post-incubation under 1% hypoxia

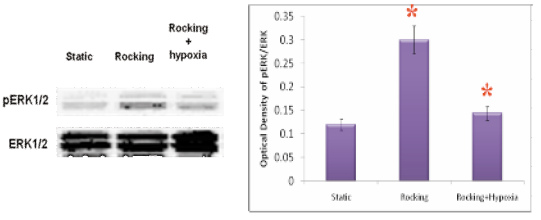

Figure 1. Rocking induces MAKP (ERK1/2) activation in MLO-Y4 osteocytes. MLO-Y4 osteocytes were rocked for 30 minutes with or without 1% hypoxia. The whole cell lysates were resolved through 10% SDS-PAGE and immunoblotted with the antibodies against the phosphorylated or total form of ERK1/2 separately. As found, rocking shear stress significantly elevated pERK1/2 level 2.5 fold without hypoxia and 1.2 fold with 1% hypoxia ($p^*<0.05$, n=3). A representative WB result is shown.

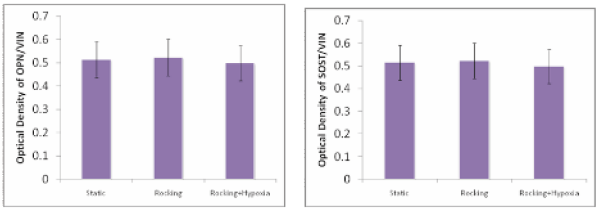

Figure 2. OPN and SOST productions were NOT significantly changed by rocking and/or hypoxia. MLO-Y4 osteocytes were rocked for 1 hour (with or without hypoxia) and post-incubated for 6 hours. The whole cell lysate was resolved through 10% SDS-PAGE and immunoblotted with antibodies against OPN and SOST. As shown, rocking did not significantly change the production of OPN and SOST in comparison to static control ($*p<0.05$, n=3).

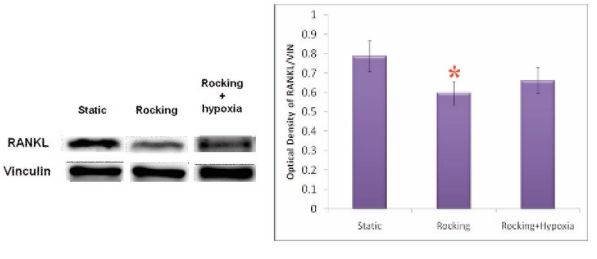

Figure 3. Rocking reduced RANKL by 24% without and by 16% with hypoxia in MLO-Y4 osteocytes. MLO-Y4 osteocytes were subjected to rocking with or without hypoxia for 1 hour, followed by a post-incubation of 6 hours. The whole cell lysate was resolved through 10% SDS-PAGE and immunoblotted against RANKL antibody. As shown, rocking reduced RANKL by 24% without hypoxia and by 16% with hypoxia ($*p<0.05$, n=3). A representative WB result is shown.

to determine protein productions of hypoxia inducible factor-1α (HIF-1α), osteopontin (OPN), sclerostin (SOST), and receptor activator of NFkB ligand (RANKL) by Western blot analysis. One-way ANOVA was used to compare rocking and non-rocking groups for each parameter with the p value being set at 0.05. As a confirmation, 1% hypoxia significantly induced HIF-1α production after 6 hours with a peak reached at 12 hours. After 30 minutes of rocking, pERK1/2/ERK1/2 was elevated 2.5 fold in rocking-treated cells without hypoxia and 1.2 fold with hypoxia (Figure 1). OPN and SOST productions were NOT significantly changed in all treatment groups (Figure 2). However, rocking

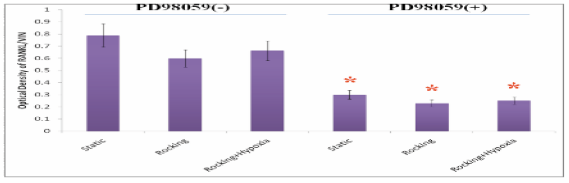

Figure 4. Blocking ERK 1/2 signaling pathway partially abolishes the inhibitory effects of hypoxia on rocking-induced reduction of RANKL in MLO-Y4 osteocytes. MLO-Y4 osteocytes were subjected to rocking with PD98059 (20 μM) for 1 hour, with or without hypoxia, followed by 6 hours of post-incubation. The cells were lysed and resolved through 10% SDS-PAGE and immunoblotted against RANKL. As shown, inhibition of ERK 1/2 significantly attenuated the rocking-induced down-regulation of RANKL by 70% (*p<0.05, n=3).

reduced RANKL by 24% (p=0.0201) without and by 16% (p=0.0316) with hypoxia (Figure 3). Inhibition of MAPK (ERK1/2) activation with PD98059 (20 μM) attenuated (by 70% down) but not abolished all the significant changes (Figure 4). Our data indicate that under hypoxia, fluid shear does not change OPN and SOST productions. Fluid shear-induced reduction of RANKL is partially independent of oxygen tension, which is partially controlled by the MAPK (ERK1/2) signaling pathway.

The author has no conflict of interest.

P-16

IGF-1 Signaling and the Skeletal Response to Mechanical Load

*R. Long
University of California, San Francisco CA, USA
E-mail: roger.long@ucsf.edu

Evidence supports the role of IGF-I signaling in mediating the skeletal response to mechanical load. Local IGF-1 production increases in response to mechanical load and, conversely, skeletal unloading causes *in vivo* and *in vitro* resistance to the effects of IGF-I. Integrins, receptors for extracellular matrix (ECM) proteins, have been shown to regulate IGF-I signaling, and this integrin/IGF-I receptor interaction may provide a mechanistic link between mechanical load and IGF-I signaling in bone. Human osteosarcoma cells (HOS) were used to study the interaction of integrins β1 and β3 and IGF-1R. These integrins were stimulated by exposure to ECM proteins and specifically targeted for knocked down by treatment with siRNA oligonucleotides. The effects of these interventions on activation of IGF-I signaling in response to IGF-I and *in vitro* mechanical loading by pulsatile fluid flow revealed that integrin stimulation augmented and targeted knock down of either integrin β1 or β3 impaired ligand and mechanical load-induced activation of IGF-1R. The sensitivity of HOS cells and the IGF-1R to mechanical load and IGF-I requires the β1 and β3 integrin receptors. The integrin regulation of IGF-1 signaling in osteoblasts allows osteoblasts to sense and respond to mechanical load, providing a link between mechanical loading, bone formation, and skeletal integrity.

The author has no conflict of interest.

P-17

A Neuronal Mechanism Regulates Modeling and Remodeling During Functional Adaptation to Cyclic Fatigue Loading

*S.J. Sample, A.P. Wilson, M. Behan, V. Miletic, P. Muir
University of Wisconsin-Madison, School of Veterinary Medicine, Comparative Orthopaedic Research Laboratory, Madison, WI, USA
E-mail: samples@svm.vetmed.wisc.edu

Bone is densely innervated and site-specific bone formation during fracture healing is correlated with sensory innervation. This study was designed to determine whether neuronal signaling regulates adaptation to fatigue loading. We used the end-loading ulna model for this study. The right ulna of 8 rats was fatigue loaded to 40% loss of stiffness (Fatigue group). Eight rats were given perineural anesthesia of the right brachial plexus with bupivacaine before loading to induce temporary neuronal blocking (BP Block+Fatigue group). 12 rats were sham-loaded (Sham group). Rats were injected with calcein after loading and 7 days later, and were euthanized at 10 days. Normalized periosteal, endosteal, and total labeled bone areas were determined in the ulnae and humeri. Resorption space number and area densities, and crack surface density were also determined. The Fatigue group showed increased bone formation in the loaded and contralateral ulnae compared to the Sham group; upon brachial plexus blocking, differences were either eliminated or diminished. Similar findings were noted in both humeri. This suggests that load-induced adaptation in this model is neuronally regulated, possibly enabling cross-talk between different appendicular long bones both within and between limbs. Brachial plexus blocking caused decreased remodeling in the fatigue-loaded ulna, suggesting that remodeling targeted at microdamage repair is also neuronally regulated. Regulation may involve the sensory innervation of bone, as sensory neuropeptides are known to influence osteoclast metabolism *in vitro*.

The authors have no conflict of interest.

P-18

Maintaining Eucalcemia Despite Prolonged Immobility and Anuria in the Hibernating Black Bear (*Ursus americanus*)

R.L Seger[1,2], R.A. Cross[3], C.J. Rosen[4], R.C. Causey[1], C.M. Gundberg[5], W.A. Halteman[6], K. Henriksen[7], W.J. Jakubas[3], R.M. Seger[8], F.A. Servello[2]
[1]Department of Animal and Veterinary Sciences, University of Maine, Orono, Maine, USA; [2]Department of Wildlife Ecology, University of Maine, Orono, Maine, USA; [3]Maine Department of Inland Fisheries and Wildlife, Bangor, Maine, USA; [4]Maine Medical Center Research Institute, Portland, Maine, USA; [5]Department of Orthopaedics and Rehabilitation, Yale University School of Medicine, New Haven, Connecticut, USA; [6]Department of Mathematics and Statistics, University of Maine, Orono, Maine, USA; [7]Nordic Bioscience, Herlev, Denmark; [8]Spectrum Medical Group, Bangor, Maine, USA.
E-mail: rita.seger@umit.maine.edu

Introduction: Mechanical signaling is an essential anabolic stimulus for bone. Mechanical unloading results in uncoupling of bone resorption and formation, with rapid, marked loss of cortical and trabecular bone. Ursine skeletal physiology has uniquely evolved to avoid net bone loss in the setting of prolonged immobility and anuria in order to prevent hypercalcemia during hibernation.

Objective: The objectives of this study were to develop a radiographic and biochemical picture of bone metabolism in active and hibernating, free-ranging black bears, and compare ursine skeletal physiology to that of humans and other species.

Methods: Forepaw radiographs of female black bears were analyzed using digital X-ray radiogrammetry of the second, third, and fourth metacarpals (DXR MCI) (Sectra Imtec, AB, Linköping, Sweden). Bone growth curves (DXR MCI *vs*. age) were constructed for an active autumn cohort (n=60) and a hibernating winter cohort (n=79) that had been in the winter den approximately 8 to 20 weeks. Serum was collected by femoral vein phlebotomy from 40 female bears active during spring and 69 female bears during winter hibernation. Serum total calcium, albumin, inorganic phosphate, creatinine, bone specific alkaline phosphatase (BSAP), tartrate resistant acid phosphatase (TRAcP), and C-terminal telopeptides of type I collagen (CTX) were measured (n=37-40 for the spring cohort, and 48-69 for the winter cohort, for individual markers).

Results: In bears less than 8.6 years-old (equivalent to mid-twenties in humans), metacarpal cortical bone mass was greater in autumn than winter bears. The maximum difference (6.4%) in metacarpal cortical bone mass occurred in bears ≤3 years-old. The difference diminished with age. The curves converged at 8.6 years, and did not differ for older individuals between autumn and winter. All bears were eucalcemic during hibernation, with age-adjusted average calcium, corrected for albumin, slightly lower in winter than spring. Relative to active bears, hibernating bears exhibited lower inorganic phosphate and age-adjusted bone specific alkaline

phosphatase (BSAP). Tartrate resistant acid phosphatase (TRAcP) did not differ with respect to activity, and creatinine was greater in hibernating bears. Elevation of age-adjusted CTX in non-lactating hibernators was within the range expected for anuric animals (2- to 2.5-fold increase). Lactating, hibernating bears exhibited a 5.5-fold greater CTX than active bears, consistent with extraction of skeletal calcium for milk production.

Discussion: Radiographic and biochemical data do not fit the pattern of unloading-induced bone loss. Radiographic findings suggest that only bears less than 9 years old lose bone from the metacarpal cortex during hibernation, whereas bears of all ages should be affected by unloading-induced bone loss. Only in bears less than 4 years old does bone loss approach the magnitude seen with mechanical unloading in other species over similar time frames. The observed pattern suggests that pre-existing osteoid may continue to mineralize during hibernation, requiring skeletal catabolism in order to maintain eucalcemia, resulting in demonstrable loss of bone until the age of peak cortical acquisition. Serum findings also do not fit the pattern of unloading-induced bone loss, because osteoclast number (measured by TRAcP) and activity (measured by CTX, corrected for anuria, in non-lactating animals) are not increased during hibernation. Bone formation (measured by BSAP) balances resorption, maintaining eucalcemia.

Conclusion: While skeletal turnover persists during ursine hibernation, unloading-induced bone loss *per se* appears not to occur. These findings suggest that the skeleton of a hibernating bear may receive a biochemical signal that it is mechanically loaded when in fact it is unloaded. Understanding the way in which signals of skeletal mechanotransduction are manipulated in the hibernating bear may shed light on this important aspect of bone metabolism.

The authors have no conflict of interest.

P-19

The Microstructural and Histological Studies of the Mandibular Cortex of Ovariectomized Monkeys

M. Tanaka[1], E. Yamashita[1], R.B. Anwar[1], H. Ohshima[2], S.Nomura[1], S. Ejiri[3]
[1]Division of Comprehensive Prosthodontics, Department of Tissue Regeneration and Reconstruction, Niigata University Graduate School of Medical and Dental Sciences, Niigata, Japan; [2]Division of Anatomy and Cell Biology of the Hard Tissue, Department of Tissue Regeneration and Reconstruction, Niigata University Graduate School of Medical and Dental Sciences, Niigata, Japan; [3]Department of Oral Anatomy, Asahi University School of Dentistry, Gifu, Japan
E-mail: mikako@dent.niigata-u.ac.jp

Objectives: The radiographic erosion of the endosteal margin of the mandibular cortex has been established as a reliable screening tool for spinal osteoporosis in postmenopausal women1. The purpose of this study was to clarify the relationship between radiographic findings and histological changes in the mandibular inferior cortices of ovariectomized monkeys.

Subjects and methods: Subjects consisted of two groups of six adult (9+ years) female cynomolgus monkeys. The experimental group was ovariectomized (OVX), with the control group receiving sham surgery (Sham). All animals were intravenously injected with calcein (8 mg/kg) 22 and 9 days before sacrifice (schedule 1-12-1-8). At the end of the experiment, all animals were sacrificed and their mandibles excised. Lumbar bone mineral densities (BMDs) and mandibular inferior cortical BMDs were measured, and dental panoramic radiographs were taken. The mandibular cortical bones were observed using microCT, confocal laser scanning microscope, and fluorescence microscopy. All procedures were performed in accordance with institutional and NIH guidelines.

Results: In the OVX group, lumbar and mandibular cortical BMDs were significantly lower than those in the Sham group. In the Sham group, the endosteal margin of the cortex was clearly defined in the panoramic radiographs. However, in the OVX group, eroded and striped shadows were detected inside the cortex, similar to those found in osteoporosis patients[1]. Histological observation of the Sham group revealed several narrow canal structures passing medio-distally through the cortex, and flattened osteoblast-like cells lining the internal surface of the canals. In the OVX group, on the other hand, several enlarged canals were found, occasionally with osteoclasts on their internal surfaces. In the Sham transverse sections, the Haversian canals were surrounded with the usual lamellar bone in the shape of concentric circles, but in the OVX group, several enlarged canals were seen with eroded surfaces, osteoid tissue, and labeling. There were significantly more canals with eroded surfaces and/or labeled surfaces in the OVX group than in the Sham group, revealing progressive bone turnover in the OVX osteons.

Conclusion: In the mandibular inferior cortex of ovariectomized monkeys, bone loss and high bone turnover were caused by estrogen deficiency. There were many enlarged canals, with bone resorptive and formative surfaces in the cortex, revealing the existence of osteon remodeling. The erosion of the endosteal margin of the mandibular cortex on the dental radiographs seems to have been caused by these enlarged canals induced by estrogen deficiency.

References

1. Taguchi A, Suei Y, Sanada Y, Ohtsuka M, Nakamoto T, Sumida H, Ohama K, Tanimoto K. Validation of dental panoramic radiography measures for identifying postmenopausal women with spinal osteoporosis. Am J Roentgenol 2004;183:1755-60.

The authors have no conflict of interest.

P-20

The Difference in Mineral Apposition Rate between Remodeling and mini-Modeling Sites in Rats' Trabecular Bone

N. Yamamoto, H.E. Takahashi, T. Shimakura
Niigata, Bone Science Institute, Niigata Japan
E-mail: nirehp.yamamoto@aiko.or.jp

Background: Remodeling is a process in which bone resorption precedes bone formation with a scalloped cement line. Mini-modeling consists of bone formation on quiescent bone surfaces with a smooth cement line. The purpose of this study is to clarify the difference of bone formation parameters in histomorphometry between remodeling sites and mini-modeling sites.

Materials and methods: Five F344 16-week-old rats were used in this study. After double labeling with calcein and tetracycline, all rats were sacrificed and L3 vertebrae and proximal tibia were taken for bone histomorphometry (magnification x 320).

Results and discussion: Baron demonstrated remodeling in rat vertebral trabecular bone (Baron R, et al. Anat Rec 208, 1984). Chow reported the presence of uncoupling in rat trabeculae, and he showed modeling ¹imini-modeling¹j in the bone formation site of growing rats (Chow JWM. Anat Rec 236, 1993). Recently, Li reported Alfacalcidol treatment induced lamellar bone bump in trabecular surface in aged male rats (Li M, et al. J Musculoskelet Neuronal Interact 4, 2004).

In this study, MAR in mini-modeling sites is significantly higher than in remodeling sites. It is supposed that the bone formation ability of individual mini-modeling sites is very strong, and it resulted in increasing bone mass. It is important to distinguish between remodeling sites and mini-modeling sites. We should evaluate the bone formation parameters in remodeling sites and mini-modeling sites separately.

The authors have no conflict of interest.

Figure 1. Mineral Apposition Rate (MAR) is higher in mini-modeling site

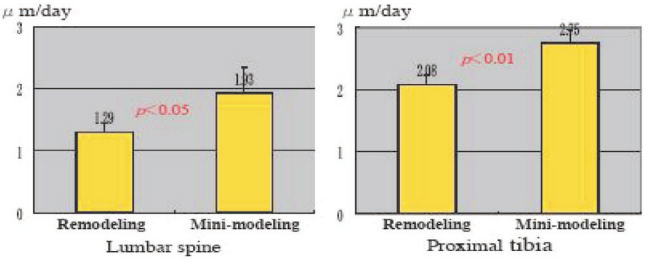

P-21

Microstructural Observation and Histological Analysis of Human Alveolar Bone Biopsy from an Implant Recipient Site

E. Yamashita[1], M. Tanaka[1], N. Sakurai[1], R.B. Anwar[1], S. Nomura[1], H. Ohshima1, S. Ejiri[2]
[1]Department of Tissue Regeneration and Reconstruction, Niigata University Graduate School of Medical and Dental Sciences, Niigata, Japan; [2]Department of Oral Anatomy, Asahi University School of Dentistry, Gifu, Japan
E-mail: emiyama@dent.niigata-u.ac.jp

Introduction: Studies on the relationship between osteoporosis and the jaw bone have been going on for more than thirty years. At present, only the finding of mandibular inferior cortical erosion on dental panoramic radiographs has been accepted as evidence of change to the jaw bone due to osteoporosis[1]. Based on this finding, an attempt was made to establish such erosion as a diagnostic tool for systemic osteoporosis[2]. Although there have been comparative studies of the relationship between systemic bone mineral density and mandibular parameters[3], there have not yet been many studies of the relationship between the systemic bone metabolism and alveolar bone quality using detailed histological research on live subjects.

Dental implants have recently become popular, even for middle-aged and elderly patients. During implant cavity preparation, the extracted alveolar bone is usually discarded. To evaluate the use of alveolar bone samples as possible diagnostic tools for osteoporosis, we examined the systemic bone metabolism and alveolar bone quality of the sample extracted from the implant recipient site.

Subject and method: The subject was a 53-year-old male, who came for implant surgery to replace his lower left first molar. Before surgery, dental X-rays, a panoramic radiograph, and CT images (slice thickness 1mm) of the mandible were taken. Biological markers of systemic bone metabolism were: the amounts of bone-specific alkaline phosphatase and osteocalcine in the blood, and deoxy-piridinoline in the urine. Calcaneus bone density was measured with an ultrasound bone densitometer (CM-200: Furuno Electricity, Tokyo, Japan). During the operation, an alveolar bone biopsy (diameter: 2mm, height: 7 mm) was obtained from the implant recipient site using a trephine bur, and then immersed in 4% formaldehyde solution. Its fine trabecular structures were observed with μCT (Elescan; Nittetsu Elex, Osaka, Japan) at slice thickness 15 μm. 3D bone morphometry was performed using TRI/3D-BON software (RATOC, Tokyo, Japan). The sample was decalcified, embedded in paraffin and cut into thin sections for HE and TRAP stainings. Histomorphometric variables were measured for an area of cancellous bone, in two sections, using a semi-automatic image analyzer system (System Supply, Nagano, Japan).

Results and discussion: μCT images of the alveolar sample demonstrated several plate-like trabeculae extending from the lingual cortical bone, although the trabeculae were not clearly visible using CT. Histological observations revealed that most of the bone surface was covered by flattened osteoblasts, although some TRAP-positive cement lines, a few osteoclasts, and cuboidal-shaped osteoblasts were also observed. Histomorphometrical results were consistent with these histological findings. The bone metabolic markers showed values within the normal range, with the bone density of the calcaneus slightly lower than the average value for the patient's age. The data obtained from the alveolar bone biopsy was therefore consistent with the state of the subject's systemic bone metabolism.

Conclusion: Our alveolar bone biopsy obtained during implant surgery was useful in gaining a detailed understanding of the state of the alveolar bone. It is hoped that in the future, more studies will be conducted on the relationship of biopsies to systemic bone metabolism, which may confirm that such biopsies may be a valuable tool for evaluating patients' systemic bone metabolism.

References

1. Taguchi A, Suei Y, Sanada M, Ohtsuka M, Nakamoto T, Sumida H, Ohama K, Tanimoto K. Validation of dental panoramic radiography measures for identifying postmenopausal women with spinal osteoporosis. AJR Am J Roentgenol 2004;183:1755–60.
2. Karayianni K, Horner K, Mitsea A, Berkas L, Mastoris M, Jacobs R, Lindh C, van der Stelt PF, Harrison E, Adams JE, Pavitt S, Devlin H. Accuracy in osteoporosis diagnosis of a combination of mandibular cortical width measurement on dental panoramic radiographs and a clinical risk index (OSIRIS): the OSTEODENT project. Bone 2007;40:223-9.
3. Amorim MA, Takayama L, Jorgetti V, Pereira RM. Comparative study of axial and femoral bone mineral density and parameters of mandibular bone quality in patients receiving dental implants. Osteoporos Int 2007;18:703-9.

The authors have no conflict of interest.